Determining unoccupied bands of layered materials by VLEED: implications for photoemission band mapping

1996 J. Phys.: Condens. Matter 8 7549

(http://iopscience.iop.org/0953-8984/8/41/005)

J. Phys.: Condens. Matter **8** (1996) 7549–7559. Printed in the UK

Determining unoccupied bands of layered materials by VLEED: implications for photoemission band mapping

V N Strocov†, H I Starnberg‡‖, P O Nilsson‡ and L J Holleboom§

† International Institute of Interphase Interactions, PO Box 1146, 194291 St Petersburg, Russia
‡ Department of Physics, Chalmers University of Technology and Göteborg University, S-412 96 Göteborg, Sweden
§ Department of Theoretical Physics, University of Lund, S-223 62 Lund, Sweden

Received 22 April 1996

Abstract. We report VLEED/TCS measurements on the layered transition metal dichalcogenide VSe_2. By combining the experimental results with simple VLEED calculations, we have been able to determine the unoccupied bands constituting the upper bands in photoemission. Our analysis reveals accurate positions of so-called coupling bands, which predominantly contribute to both electron transmission and photoemission. Better knowledge about these bands may substantially improve the accuracy of valence band mapping, particularly in studies of layered materials like VSe_2, as the upper bands of these are too complicated to be well approximated by free-electron-like bands. We discuss in some detail the connection between VLEED and photoelectron spectroscopy, and we obtain for the first time a detailed recipe for $k_\perp$-resolved band mapping, with utilization of VLEED results. Some previous photoemission results are re-examined in the light of our present findings, and the power of combined VLEED/photoemission studies is stressed.

1. Introduction

The layered transition metal dichalcogenides (TMDCs) crystallize as a stack of layers, each consisting of a sheet of transition metal atoms sandwiched between two sheets of chalcogen atoms. With strong bonding within each layer, but much weaker interactions between the layers, these materials are characterized by highly anisotropic physical properties, and many interesting phenomena, associated with reduced dimensionality, have been observed [1]. Of particular interest is the possibility of inserting foreign atoms and molecules between the layers. This process, known as intercalation, can be used to modify the characteristics of TMDCs in a controllable way, and is of great interest in fundamental studies, as well as for practical applications [1, 2].

As for crystalline solids in general, the electronic band structure is a key concept in the understanding of the properties of TMDCs. Extensive studies by means of angle-resolved photoelectron spectroscopy (ARPES) and related techniques have provided detailed knowledge about the electron band dispersion parallel to the surface [2–7]. However, mapping of the perpendicular dispersion $E(k_\perp)$ requires some knowledge about the dispersion of the unoccupied upper bands. For many materials, satisfactory results have been obtained by presuming free-electron-like upper bands, but for the TMDCs this approach has been less successful, as their upper bands are too complicated [8]. The determination of

‖ Author to whom any correspondence should be addressed.

0953-8984/96/417549+11$19.50

TMDC upper bands, suitable for ARPES band mapping, therefore presents a challenge of principal importance.

A promising approach for electronic band determination above the vacuum level is to measure the electron reflectivity $R(E)$ by means of very-low-energy electron diffraction (VLEED), as reviewed in [9]. Typically $R(E)$ is measured for electron energies E in the range 0–30 eV relative to the vacuum level. A particularly beneficial feature of VLEED is that it probes exactly those upper bands which constitute the final bands in ARPES [9–12].

We here report VLEED measurements on VSe_2, which is an extensively studied TMDC adopting the simple 1T-CdI_2 structure [1, 5, 6]. By combining the experimental results with simple VLEED calculations, we have been able to determine upper bands relevant for ARPES band mapping. We provide an extensive discussion on how to best exploit the present results in ARPES studies. Some previous ARPES results for VSe_2 [13] are re-examined in the light of our present findings.

2. VLEED band determination

2.1. Principles of VLEED band mapping

The elastic electron reflectivity $R(E)$ of a single-crystal surface is governed by the matching of exterior plane waves to the Bloch waves of the crystal interior, under conservation of both energy E and parallel momentum $\boldsymbol{K}_\parallel$ [14–16]. Among these Bloch waves, only those ones which have dominant Fourier components resembling the incident plane wave (so-called coupling bands) are significantly excited. The matching thus provides a direct link between $R(E)$ and the coupling bands [17–19].

Previously the feasibility of detailed VLEED band mapping has been demonstrated [18–20]. The upper bands were here obtained using the no-absorption approximation, which neglects the electron absorption. An important concept within this approximation is that of critical points (CPs), which are defined as points where $\partial E/\partial k_\perp$ undergoes sharp changes, or vanishes at the band-gap edges. It was found that each CP of a coupling band is associated with a sharp change of the wavefunction excited in the crystal. This gives rise to a rapid change of $R(E)$, and consequently an extremum in $\mathrm{d}R/\mathrm{d}E$. By comparing experimental and calculated $\mathrm{d}R/\mathrm{d}E$ extrema, the empirical CP positions were found. From their dispersion upon variation of $\boldsymbol{K}_\parallel$, complete bands in symmetry planes of the Brillouin zone were mapped.

Recently the principles of VLEED band mapping have been extended to the excited-state description [21]. Finite electron absorption V_i results in smooth-looking excited-state bands $E(\mathrm{Re}\,\boldsymbol{k})$ without band gaps, but there are nonetheless well-defined irregularity points (IPs), which are linked to the $\mathrm{d}R/\mathrm{d}E$ extrema in the same way as the CPs of no-absorption bands. In analogy with the no-adsorption case, the experimental positions of the coupling-band IPs were therefore obtainable from VLEED data. In addition, the empirical coupling bands were obtained as a whole by fitting a reference band calculation to the experimental IPs. It was also found that the no-absorption CPs evolve into IPs as the absorption V_i is introduced, without significant changes of their energy. This justifies the application of the no-absorption approximation when V_i is small, provided that the CP energies obtained are actually understood as corresponding IP energies.

2.2. Experimental details

Our VLEED data were obtained by measuring the current absorbed by the sample. This technique, also known as target current spectroscopy (TCS) [20, 22], probes the transmission $T(E)$ of the surface, and the total reflectivity is readily obtained as $R(E) = 1 - T(E)$. Formally, the total reflectivity includes a contribution from inelastic electrons, but all of the fine structure is due to the elastic component, provided that the inelastic contribution is rather featureless.

The experimental set-up, which has been described elsewhere [20], was a conventional four-grid LEED unit, operated in the retarding-field mode. Normal operation of the electron gun was achieved by biasing its exit electrode to +300 eV. The grids were biased to +100 V. With the sample at ground potential, the electrons were retarded to low primary energies E by the retarding field between the gun and the sample. By this technique, the spot diameter could be kept less than 2 mm down to $E = 5$ eV. However, for a constant sample rotation angle α, the retarding field caused the incidence angle (and $\boldsymbol{K}_\parallel$) to depend on the energy E [9, 20]. The dependence of $\boldsymbol{K}_\parallel$ on E was determined empirically by fitting the function $K_\parallel(\alpha, E) = C_1\alpha^{1/2} + C_2\alpha + C_3\alpha E$ to experimental points with well-defined $\boldsymbol{K}_\parallel$ [23]. The accuracy of the $K_\parallel$-determination was 0.03 Å^{-1}.

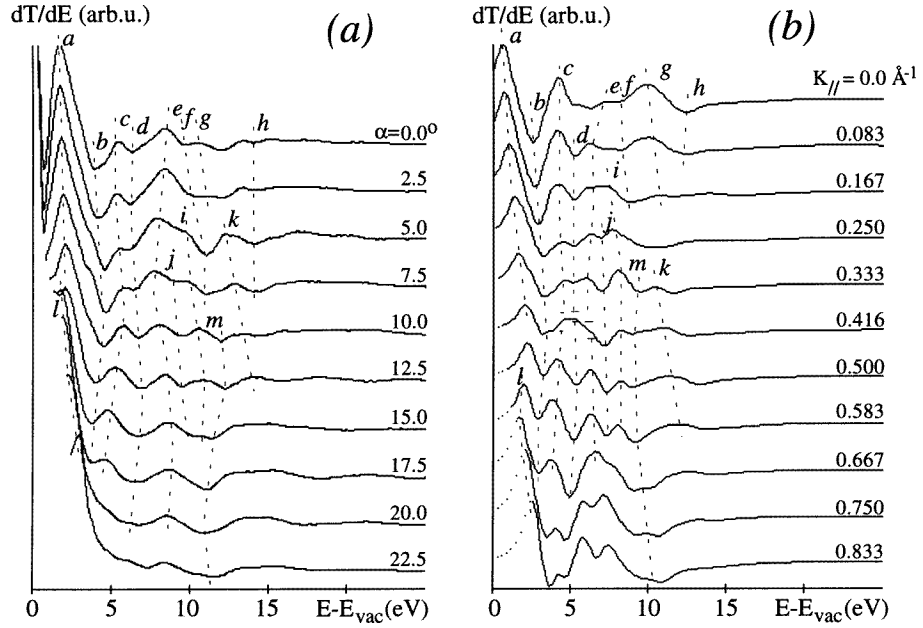

Figure 1. dT/dE spectra, obtained under variations of incidence $\boldsymbol{K}_\parallel$ along the ΓK line of the Brillouin zone. (*a*) Experimental spectra, with the angle of sample rotation α indicated. The primary peaks at the onset energy are excluded. (*b*) Calculated spectra with $K_\parallel$ indicated. Below the onset energy $E = \hbar^2 K_\parallel^2/2m$ the spectra are shown by rarefied points. Corresponding structures of (*a*) and (*b*) are labelled with the same letters.

The clean surface of VSe_2, prepared by cleavage *in situ*, produced a sharp LEED pattern. The sample was azimuthally oriented so that $\boldsymbol{K}_\parallel$ was scanned along the ΓK line as α was increased. Figure 1(*a*) shows the experimental spectra measured for different values of α. Throughout this paper we give the energy relative to the vacuum level, with the workfunction

determined to be 5.6 ± 0.3 eV. The spectra are presented as $\mathrm{d}T/\mathrm{d}E$ plots, to emphasize the fine structure. The apparent angular dispersion of the spectral structures confirms their elastic origin. (In principle, the spectra could also exhibit inelastic features [22]. However, inelastic features due to interband transitions should rather reflect the $\boldsymbol{k}$-integrated density of states, and therefore not depend appreciably on the incidence angle. Plasmon excitation features at low energies, due to $\boldsymbol{q}$-space integration, also should not show significant angle dependence.) Above $E_{thr} \approx 16$ eV the spectral structures are smoothed out due to the sharp increase of the electron absorption at the plasmon threshold. $\mathrm{d}T/\mathrm{d}E$ extrema were stable within ± 0.25 eV upon tuning the experimental settings, which gives the experimental accuracy.

2.3. Computational procedure

The ground-state band structure of VSe_2 was calculated by the LAPW method within the LDA-DFT approximation. The potential was of non-muffin-tin type and generated self-consistently. $T(E)$ curves were calculated with a modified conducting-Fourier-component (CFC) approximation [17, 18], employing the Fourier expansion of the bulk wavefunctions between the ion cores. For this purpose the plane-wave parts of the LAPW wavefunctions were utilized, represented as an expansion

$$\sum_{\boldsymbol{G}} C_{\boldsymbol{G}} \exp[\mathrm{i}(\boldsymbol{k} + \boldsymbol{G}) \cdot \boldsymbol{r}].$$

The partial transmission T_i of any Bloch wave is then obtained as

$$T_i = \sum_{\boldsymbol{G}'} \sqrt{\frac{2\,\mathrm{sgn}(k_\perp + G'_\perp)}{1 + \hbar|k_\perp + G'_\perp|/\sqrt{2mE}}} C^2_{\boldsymbol{G}'}$$

where the sum is over the reciprocal vectors $\boldsymbol{G}'$ satisfying $\boldsymbol{k}_\parallel + \boldsymbol{G}'_\parallel = \boldsymbol{K}_\parallel$, and $C_{\boldsymbol{G}'}$ are the amplitudes of the corresponding so-called conducting components in the Fourier expansion expansion above. The denominator stands for a one-dimensional simulation of the step-like surface barrier. The total $T(E)$ is approximated as the largest partial T_i among all propagating Bloch waves available for given E and $\boldsymbol{K}_\parallel$:

$$T(E) = \max_{E, \boldsymbol{K}_\parallel} \{T_i\}.$$

Values of partial T_i were calculated with $k_\perp$ sampled in steps of $0.01|\Gamma A|$, and the largest were accumulated in 0.1 eV wide energy bins to produce the total $T(E)$.

The electron absorption was simulated by Lorentzian convolution of $T(E)$ with the half-width equal to the optical potential V_i, and by division of $T(E)$ by V_i. The energy dependence of V_i was modelled as a linear contribution from the electron–electron scattering, with a Fermi–Dirac-like step added at the plasmon threshold E_{thr} [4, 24]:

$$V_i(E) = 0.5 + 0.04E + \frac{2.5}{1 + \exp[-(E - E_{thr})/2.0]}\ (\mathrm{eV}).$$

From the (valence) plasmon energy $\hbar\omega \approx 21.5$ eV, typical for TMDCs [25], and the experimental value for the workfunction we estimated that $E_{thr} \approx 16$ eV. Other numerical parameters were assessed by comparison with the experimental spectra.

Figure 1(*b*) shows the calculated plots $\mathrm{d}T/\mathrm{d}E$ for various $\boldsymbol{K}_\parallel$ along ΓK.

2.4. Comparison of experimental and calculated spectra

The calculated spectra in figure 1(*b*) are strikingly similar to the experimental ones in figure 1(*a*), with an almost one-to-one correspondence between their detailed features. This is stressed in figure 1 by labelling corresponding experimental and calculated $\mathrm{d}T/\mathrm{d}E$ extrema with the same letters. The agreement is particularly remarkable in view of the simplified computational procedure, and the experimental problems at very low electron energies. Some amplitude discrepancies are typical for the CFC approximation [18]. For larger $\boldsymbol{K}_{\parallel}$-values the experimental spectra are smoother, due to the enhanced electron absorption V_i at grazing incidence.

As a general trend, the experimental $\mathrm{d}T/\mathrm{d}E$ extrema are shifted by 1–2 eV to higher energy relative to their calculated counterparts. This reflects the fact that the experimental CPs are shifted from their calculated ground-state energies by the self-energy correction $\Delta\,\mathrm{Re}\,\Sigma$ [21, 26]. As a function of energy, $\Delta\,\mathrm{Re}\,\Sigma$ was least-squares fitted as $\Delta\,\mathrm{Re}\,\Sigma = 0.16E + 0.64$ (eV) with the RMS error = 0.5 eV. However, no unambiguous dependence of the self-energy correction upon $\boldsymbol{K}_{\parallel}$ was found within the experimental accuracy, despite of the high anisotropy of VSe_2.

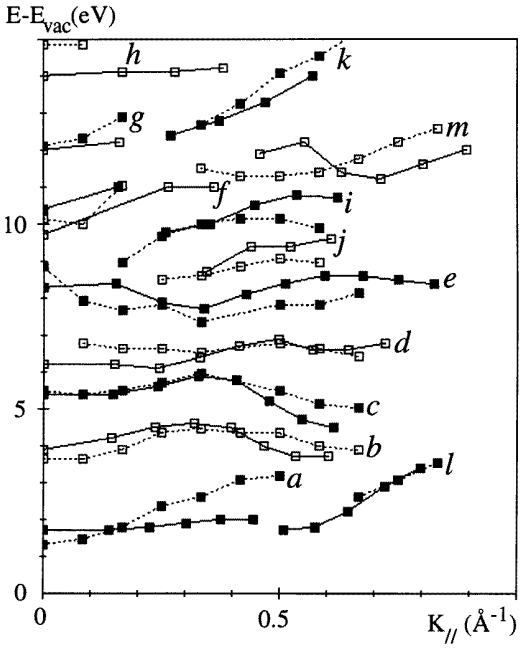

Figure 2. The dispersion of experimental (dashed lines) and calculated (solid lines) $\mathrm{d}T/\mathrm{d}E$ extrema with $\boldsymbol{K}_{\parallel}$ along the ΓK line. Open and filled squares stand for minima and maxima, respectively. The calculated dispersions are shifted to higher energies by the empirical self-energy correction $\Delta\,\mathrm{Re}\,\Sigma = 0.16E + 0.65$ (eV).

Figure 2 shows the dispersions of the experimental $\mathrm{d}T/\mathrm{d}E$ extrema, superimposed on the dispersions of the calculated ones. The latter are corrected using the above expression for $\Delta\,\mathrm{Re}\,\Sigma$. The agreement is striking, and the remnant discrepancies, particularly near $\boldsymbol{K}_{\parallel} \approx 0.5$ Å^{-1}, are attributed mainly to the perturbation of very-low-energy electron trajectories from stray electrostatic and magnetic fields, and to misalignments of the electron

optics. In addition, with a strong retarding field present between the gun and the sample, we could not compensate for the influence of the grounded manipulator [20], which gave rise to a small energy-dependent deviation of the electron beam by 1–2° in the vertical plane, corresponding to $\Delta K_{\parallel} \approx 0.05$–$0.1$ Å^{-1} according to extensive ray-tracing calculations [27]. The spurious structure at 12 eV in the normal-incidence spectrum is most probably caused by this.

2.5. The band-mapping procedure

The experimental upper bands were found in the no-absorption approximation [21], using our ground-state band calculations. This approximation is well justified below the plasmon threshold because of the absorption V_i being weak (≈1 eV), as compared to typical energy separations between band-structure features.

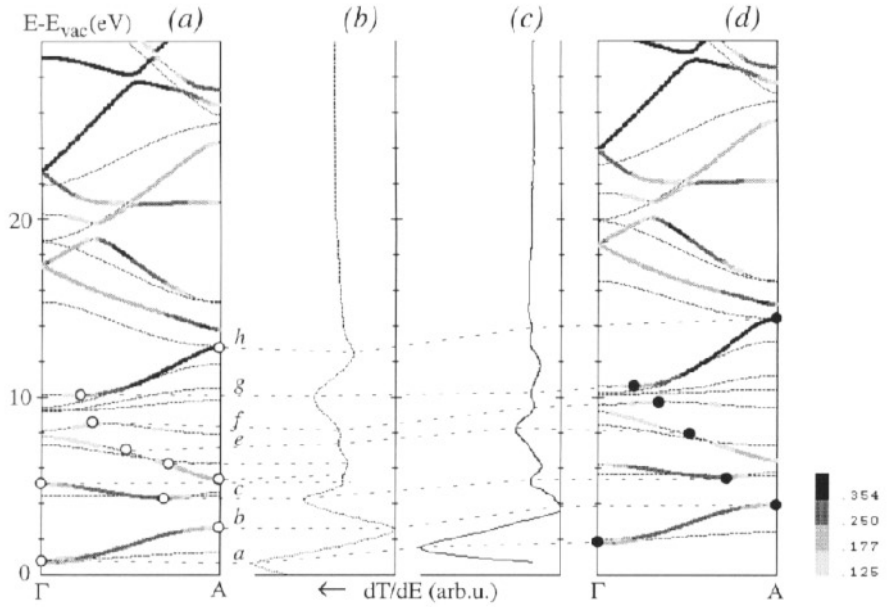

Figure 3. (*a*) The calculated reference band structure along ΓA. The partial transmission coefficients T_i of the bands are indicated by the grey-scale. The CPs of the coupling bands are shown (open dots). (*b*) The corresponding calculated normal-incidence $\mathrm{d}T/\mathrm{d}E$ spectrum. Its extrema are connected with the related CPs of the calculated bands. (*c*) The experimental normal-incidence $\mathrm{d}T/\mathrm{d}E$ spectrum. The spurious structure near $E = 12$ eV is due to the uncompensated vertical deviation of the electron beam, and the structure near 6 eV is smoothed by the beam divergence. (*d*) The experimental band structure, empirically fitted to the experimental CPs (filled dots). The experimental CPs were mapped by shifting the calculated ones, so that the energies of the relevant $\mathrm{d}T/\mathrm{d}E$ extrema match their experimental positions. Energies of mapped CPs are accurate within ±0.25 eV.

Using our LAPW-based calculation as a reference, we started by establishing the correspondence between the band structure and the $\mathrm{d}T/\mathrm{d}E$ curves. This is illustrated in figure 3 for the case of normal incidence. The calculated bands in figure 3(*a*) are drawn in different shades of grey according to their partial transmissions T_i. The coupling bands, which dominate the total $T(E)$, are those having the largest values of T_i. Each CP of the

coupling bands is associated with a sharp change of the wavefunction excited in the crystal, and therefore produces an extremum in the dT/dE curve, as can be seen in figure 3(*b*). The non-coupling bands are invisible in the dT/dE curves because of their negligible transmissions T_i. Closer to the plasmon threshold the one-to-one correspondence is lost, as the increasing absorption V_i mixes up the features of adjacent CPs, and finally the dT/dE extrema are smoothed out by V_i exceeding 3 eV.

The calculated dT/dE curves were then compared with the experimental ones, as exemplified in figure 3(*c*). Corresponding extrema are designated with the same letters. (The calculated structure near 6 eV due to three close CPs is strongly $\boldsymbol{K}_\parallel$-dispersive, and was smoothed in the experimental spectra due to the divergence of the electron beam. The structure near 12 eV is probably due to the uncompensated $\Delta\boldsymbol{K}_\parallel$ in the vertical plane, which splits the otherwise degenerate ΓA band near 11 eV in figure 3(*a*).) First the experimental CPs were mapped by correcting their calculated position with the energy difference ΔE between the corresponding experimental and calculated dT/dE extrema. Then the experimental bands as a whole (figure 3(*d*)) were obtained by fitting to the CPs determined. For this purpose we shifted the calculated bands by an energy-dependent ΔE linearly varying between the fixed experimental CPs. Above the plasmon threshold, we had no experimental points, but applied tentatively the average energetic shift $\Delta E = 1.2$ eV, obtained from all of the experimental CPs above 10 eV. Note that our experimental bands appear very different from a free-electron parabola placed at the valence band bottom, which previously was assumed [5].

The experimental bands along off-symmetry directions were similarly determined, with the experimental energies of CPs determined by linear interpolation in $\boldsymbol{K}_\parallel$. Due to the lifting of the degeneracy, the band structure appears here extremely involved, with the coupling bands divided into pieces, each narrower than $|\Gamma A|/2$.

3. Implications in photoemission

3.1. General principles

The one-step theory of photoemission [10, 11, 28] gives the photocurrent $I_\nu(E)$ from the νth initial state Φ_ν as

$$I_\nu(E) \propto |\langle \Phi^{L*} | \hat{\boldsymbol{A}} \cdot \hat{\boldsymbol{p}} | \Phi_\nu \rangle|^2$$

where $\hat{\boldsymbol{A}}$ is the screened vector potential of the electric field, $\hat{\boldsymbol{p}}$ is the momentum operator, and Φ^{L*} is exactly the LEED wavefunction, which would be excited in the crystal by incident electrons coming from the photoemission detector.

If the absorption V_i is modest and if hole lifetime effects can be neglected, the expression for the photoemission current dI_ν from the νth initial state in the energy interval dE may be simplified to [10, 28, 29]

$$dI_\nu \propto dE \left(\frac{1}{v_\nu}\right) \sum_{n,n'} |T_n|^2 \, |\beta_{\nu n'}|^2 \, |M_{nn'}|^2 \, |\Delta_{nn'}|^2$$

where n enumerates the damped Bloch waves with complex wavevectors $k_{\perp n}$, which constitute the final state Φ^{L*}; T_n are their excitation amplitudes found from a LEED calculation; $\beta_{\nu n'}$ are the expansion coefficients of the νth initial state Φ_ν over the Bloch waves with their complex wavevectors $k_{\perp n'}$; $1/v_\nu$, where v_ν is the group velocity $(\partial E/\partial \operatorname{Re} k_\perp)/\hbar$ of the Bloch wave in the initial state propagating towards the surface, is proportional to the associated one-dimensional DOS; $M_{nn'}$ is the dipole matrix element of

the vector potential $\hat{\boldsymbol{A}}$ between the n'th initial and nth final-state Bloch waves; and $|\Delta_{nn'}|^2$ is a Lorentzian describing the relaxed $k_\perp$-conservation:

$$|\Delta_{nn}|^2 = \frac{1}{(\mathrm{Re}\, k_{\perp n} - \mathrm{Re}\, k_{\perp n'})^2 + (\mathrm{Im}\, k_{\perp n})^2}.$$

The maximum of $|\Delta_{nn'}|^2$ corresponds to the direct $k_\perp$-conserving transition with $\mathrm{Re}\, k_{\perp n} = \mathrm{Re}\, k_{\perp n'}$, and the half-width $\mathrm{Im}\, k_{\perp n}$ is determined by the final-state absorption V_i and by the slope $\partial E_n/\partial\, \mathrm{Re}\, k_{\perp n}$ (proportional to the group velocity v_n) of the nth final-state band through

$$\mathrm{Im}\, k_{\perp n} = \frac{V_i}{\partial E_n/\partial\, \mathrm{Re}\, k_{\perp n}}.$$

Provided that the absorption V_i is weak, a photoemission spectrum appears as a superposition of Lorentzians centred on the $k_\perp$-conserving positions, with their amplitudes determined by the factors $1/v_\nu$, T_n, $\beta_{\nu n'}$, and the matrix elements $M_{nn'}$.

Two conditions have to be fulfilled to allow for $k_\perp$-resolved band mapping.

(i) The Lorentzian widths should be small, so that the variations of the factors $1/v_\nu$, T_n, $\beta_{\nu n'}$, $M_{nn'}$ across their profiles do not shift their maxima appreciably from the positions corresponding to $k_\perp$-conservation. In $\boldsymbol{k}$-space, variations of these factors typically occur over distances comparable with the Brillouin zone perpendicular dimension $k_\perp^{BZ}$. Therefore, this condition may be formulated as $\mathrm{Im}\, k_{\perp n} \ll k_\perp^{BZ}$.

(ii) Of the Bloch waves constituting the final state, only one should have the dominant excitation amplitude T_n, so $k_\perp$ for the transition is uniquely determined. Otherwise, analysis of the factors $1/v_\nu$, $\beta_{\nu n'}$, and $M_{nn'}$ is needed.

3.2. The relevance of VLEED band mapping for photoemission

The crucial point for the applications of VLEED in photoemission is that the final state of the photoemission Ψ^L is exactly a time-reversed LEED wavefunction, as we have pointed out above. In particular, the coupling bands were defined in VLEED as those effectively matching the incident plane wave through their maximal partial transmission T_i. As their T_i is a good approximation for the excitation amplitude T_n, exactly the same bands with maximal T_n predominantly contribute to the photocurrent (provided that the factors $1/v_\nu$, $\beta_{\nu n'}$, $M_{nn'}$ do not vanish). Thus, the experimental band fitting based on VLEED provides the dominant, or coupling, upper bands of photoemission. Larger errors are tolerable for the non-coupling bands, which remain invisible in both VLEED and photoemission.

3.3. Upper bands of VSe_2 suitable for $k_\perp$-resolved band mapping

We have analysed the experimental upper bands (figure 3(*d*)) to determine where the conditions for $k_\perp$-resolved band mapping are fulfilled. From 29 eV down to 24 eV there is a single coupling band. However, $V_i \approx 4$ eV results in the $k_\perp$-broadening $\mathrm{Im}\, k_\perp \approx 0.8|\Gamma\mathrm{A}|$, which is too large. From 24 eV to 16 eV there are two available final bands. However, their T_i differ only by a factor of 1.5, which makes the $k_\perp$-determination ambiguous without an amplitude analysis. From 16 eV to 15 eV a single coupling band exists, but we expect a large contribution from the evanescent Bloch wave corresponding to the band gap at $k_\perp = |\Gamma\mathrm{A}|$.

V_i drops sharply below the plasmon threshold. The coupling band going from 14 eV down to 10 eV appears suitable for band mapping. The $k_\perp$-broadening of this band seems

somewhat large ($\approx 0.23|\Gamma A|$), but we suspect that the function $V_i(E)$ employed in our calculations was slightly overestimated. Also, we found with a simplified model that the excited-state smoothing of the coupling bands tends to increase their slope $\partial E/\partial k_\perp$ close to the band gaps, thereby reducing the $k_\perp$-broadening†. An explicit excited-state calculation is needed to clarify this point.

The split band between 9 eV and 6.5 eV also provides suitably small $k_\perp$-broadening ($\approx 0.31|\Gamma A|$). Although this band may be of use for band mapping, we cannot exclude strong photoemission from evanescent Bloch waves in the band gap at $k_\perp = 0$. Below 6 eV, the bands are hardly accessible in a photoemission experiment.

The experimental bands along off-symmetry directions were also analysed. Here the coupling bands are divided into short pieces, each rather flat, which results in inappropriate $k_\perp$-broadening. However, simulation of excited-state effects joined them to continuous lines with increased slope $\partial E/\partial k_\perp$, sufficient for band mapping below the plasmon threshold.

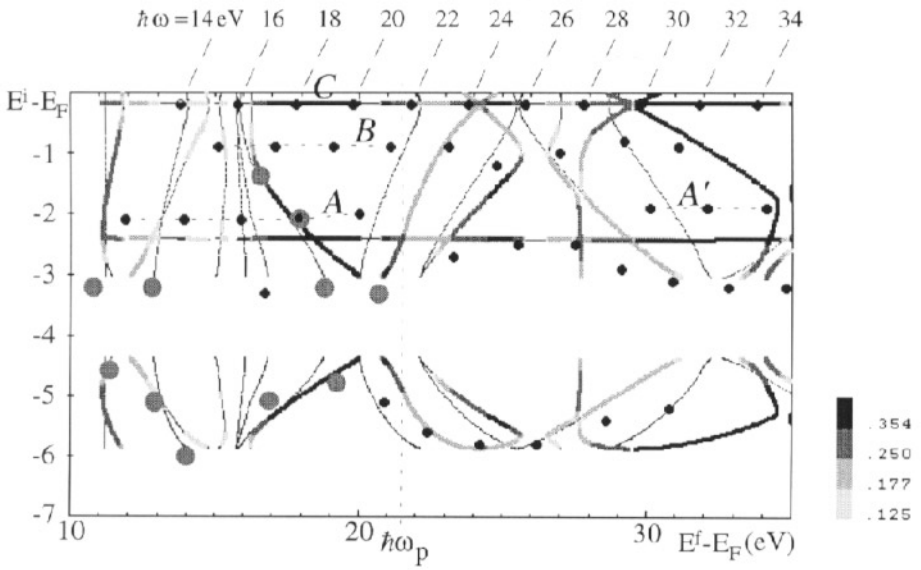

Figure 4. A structure plot for the normal photoemission, constructed from the LAPW-calculated lower bands and the upper bands derived from VLEED data. The partial transmissions T_i of the upper states are indicated by the grey-scale. Peak positions of the experimental EDCs are shown as black dots, except those corresponding to direct transitions, which are shown as large grey dots.

3.4. Testing of the experimental upper bands

Our results were tested with the available experimental photoemission data on VSe_2 [13]. Figure 4 shows a structure plot, constructed from the upper bands found by VLEED, figure 3(*d*), as final bands, and the LAPW-calculated initial bands‡. The points in this plot

† Our model employed tentative guesses of the real lines, which connect the experimental coupling bands across their band gaps. Then the overall dependence $k_\perp(E)$, plotted in the extended zone scheme, was smoothed by a Lorentzian with half-width $V_i(E)$.

‡ We have also tested the excited-state upper bands obtained with our simplified model, but the available photoemission data points are too coarse for us to decide whether the description is improved.

are pairs of final band energies $E^f - E_F$ and initial band energies $E^i - E_F$ with the same $k_\perp$, which corresponds to direct transitions. The amplitudes of the relevant photoemission peaks are determined by the factors $1/v_v$, $\beta_{vn'}$, $M_{nn'}$, and T_n. The latter factor, approximated by T_i, is indicated with a grey-scale. Points of vanishing T_i should vanish also in photoelectron spectra.

The peaks of the experimental photoemission EDCs are shown by grey and black dots. One recognizes the dispersionless initial Se $4p_{x,y}$ bands (A and A′), and the V 3d band (C). The weak feature B is possibly a Frenkel defect state [30], or a multielectron satellite of the V 3d band. However, below the plasmon threshold, all dispersive features (grey dots) are in very reasonable agreement with the experimental upper bands, with a single exception due to the high DOS at the bottom of the Se $4p_z$ band. (At final energies from $E^f - E_F = 12$ eV to 21 eV the upper bands are fairly close to a free-electron parabola with the bottom about 10 eV above E_F, which was proposed in [13] as the best fit to the photoemission experiment. However, such a fit is relevant only locally, strongly depending on the energy and particularly on $\boldsymbol{k}_\parallel$.) The band-gap emission near 15 eV is probably hidden by the large emission from the V 3d band.

Obvious disagreements above the plasmon threshold occur for several reasons. Firstly, a large absorption V_i strongly modifies the no-absorption bands employed by us. Secondly, the photoemission peaks are shifted from their $k_\perp$-conserving positions due to substantial variation of the initial band DOS $1/v_v, T_n, \beta_{vn'}$ and $M_{nn'}$ across the broad $k_\perp$-conserving Lorentzian (half-width $\approx 0.8|\Gamma\mathrm{A}|$) [31]. Above $E^f - E_F = 30$ eV the $k_\perp$-broadening is becoming so large that any dispersion of the photoemission peaks disappears. Thirdly, closer to the plasmon threshold appreciable shifts appear due to the local field effects [32]. An explicit analysis, based on the one-step photoemission theory and including the electron absorption V_i, is needed here.

4. Conclusions

4.1. VLEED mapping of unoccupied states

The structure of unoccupied upper bands of layered VSe_2 has been determined, using reference LAPW band calculations in conjunction with Fourier composition analysis of the wavefunctions. We have identified the coupling bands, which dominate both electron transmission and photoemission. Then the position of these bands has been unambiguously determined from VLEED/TCS experimental data. The experimental bands differed markedly from commonly used free-electron parabolas, and were shifted to higher energy in comparison with the reference ground-state calculation. The agreement with the available photoemission data is very encouraging.

We want to stress the need for excited-state calculations of the reference band structure to further improve the accuracy of the experimental upper bands.

4.2. A recipe for $k_\perp$-resolved photoemission band mapping

Analysis of the experimental upper bands has allowed us to formulate the following experimental conditions for a more detailed $k_\perp$-resolved photoemission band mapping of VSe_2.

(i) The final-state energies should be between 6 eV and 14.5 eV, where the two steep coupling bands provide a satisfactorily small $k_\perp$-broadening. This corresponds to photon

energies $\hbar\omega$ from 15 eV to 24 eV. Above the plasmon threshold ($\approx$16 eV) the mapping is prohibited by strong $k_\perp$-broadening comparable to the Brillouin zone dimension.

(ii) As the above-mentioned bands cross the Brillouin zone on variations of $\hbar\omega$ of only 2–6 eV, the need for sufficient sampling of the occupied bands requires the $\hbar\omega$-steps to be kept smaller than 0.2–0.5 eV.

(iii) Determination of $k_\perp$ should employ the empirical final band dispersion derived from VLEED data.

We want to stress again the power of combined VLEED/photoemission studies for accurate $k_\perp$-resolved band mapping. This is particularly important for non-metal materials, which are generally characterized by strong deviations of their unoccupied bands from free-electron-like behaviour.

References

[1] Friend R H and Yoffe A D 1987 *Adv. Phys.* **36** 1
[2] Brauer H E, Starnberg H I, Holleboom L J and Hughes H P 1995 *Surf. Sci.* **331–333** 419
[3] Johnson M T, Starnberg H I and Hughes H P 1986 *J. Phys.: Condens. Matter* **19** L451
[4] Pehlke E, Schattke W, Andersson O, Manzke R and Skibowski M 1990 *Phys. Rev.* B **41** 2982
[5] Law A R, Andrews P T and Hughes H P 1991 *J. Phys.: Condens. Matter* **3** 813
[6] Claessen R, Schäfer I and Skibowski M 1990 *J. Phys.: Condens. Matter* **2** 10 045
[7] Langlais V, Belkhir H, Themlin J-M, Debever J-M, Yu L-M and Thiry P A 1995 *Phys. Rev.* B **52** 12 095
[8] Pehlke E and Schattke W 1987 *J. Phys. C: Solid State Phys.* **20** 4437
[9] Strocov V N 1995 *Int. J. Mod. Phys.* B **9** 1755
[10] Feibelman P J and Eastman D E 1974 *Phys. Rev.* B **10** 4932
[11] Pendry J B 1976 *Surf. Sci.* **57** 679
[12] Nilsson P-O, Kanski J and Larsson C G 1980 *Solid State Commun.* **36** 111
[13] Starnberg H I, Brauer H E, Nilsson P O, Holleboom L J and Hughes H P 1994 *Mod. Phys. Lett.* **8** 1261
[14] Capart G 1969 *Surf. Sci.* **13** 361
[15] Pendry J B 1974 *Low Energy Electron Diffraction* (London: Academic)
[16] Jaklevic R C and Davis L C 1982 *Phys. Rev.* B **26** 5391
[17] Strocov V N 1991 *Solid State Commun.* **78** 845
[18] Strocov V N and Komolov S A 1991 *Phys. Status Solidi* b **167** 605
[19] Strocov V N 1993 *Int. J. Mod. Phys.* B **7** 2813
[20] Strocov V N and Starnberg H I 1995 *Phys. Rev.* B **52** 8759
[21] Strocov V N, Starnberg H I and Nilsson P O 1996 *J. Phys.: Condens. Matter* **8** 7539
[22] Komolov S A 1992 *Total Current Spectroscopy of Surfaces* (Philadelphia, PA: Gordon and Breach)
[23] Strocov V N and Starnberg H I 1995 *Solid State Commun.* **96** 659
[24] Smith A E 1984 *Phys. Status Solidi* b **123** 619
[25] Bell M G and Liang W Y 1977 *Adv. Phys.* **25** 53
[26] Goldmann A, Altmann W and Dose V 1991 *Solid State Commun.* **79** 511
[27] Strocov V N and Starnberg H I 1996 to be published
[28] Grandke T, Ley L and Cardona M 1978 *Phys. Rev.* B **18** 3847
[29] Jepsen D W, Himpsel F J and Eastman D E 1982 *Phys. Rev.* B **26** 4039
[30] Pehlke E and Schattke W 1987 *Z. Phys.* B **66** 31
[31] Pehlke E and Schattke W 1989 *Solid State Commun.* **69** 419
[32] Bödicker A, Leventi-Peetz A and Schattke W 1996 *J. Electron Spectrosc.* **78** 481